JACS
JOURNAL OF THE AMERICAN CHEMICAL SOCIETY
Communication
Cite This: J. Am. Chem. Soc. 2018, 140, 570−573
pubs.acs.org/JACS

Negative Differential Conductance in Polyporphyrin Oligomers with Nonlinear Backbones

Guowen Kuang,[†] Shi Zhang Chen,[‡] Linghao Yan,[†] Ke Qiu Chen,*[,‡] Xuesong Shang,[§] Pei Nian Liu,*[,§] and Nian Lin*[,†]

[†]Department of Physics, The Hong Kong University of Science and Technology, Hong Kong, China
[‡]Department of Applied Physics, School of Physics and Electronics, Hunan University, Changsha 410082, China
[§]Shanghai Key Laboratory of Functional Materials Chemistry and School of Chemistry & Molecular Engineering, East China University of Science and Technology, Meilong Road 130, Shanghai 200237, China

Supporting Information

ABSTRACT: We study negative differential conductance (NDC) effects in polyporphyrin oligomers with nonlinear backbones. Using a low-temperature scanning tunneling microscope, we selectively controlled the charge transport path in single oligomer wires. We observed robust NDC when charge passed through a T-shape junction, bistable NDC when charge passed through a 90° kink and no NDC when charge passed through a 120° kink. Aided by density functional theory with nonequilibrium Green's functions simulations, we attributed this backbone-dependent NDC to bias-modulated hybridization of the electrode states with the resonant transport molecular orbital. We argue this mechanism is generic in molecular systems, which opens a new route of designing molecular NDC devices.

Negative differential conductance (NDC) has become the basis of many electronic devices.[1,2] In the past two decades, the NDC effect in molecular systems has been extensively studied drive by the fast development of molecular electronics.[3] It has been proposed that NDC can be caused by sharp density of states of the electrode,[4] molecule-electrode coupling,[5] molecular vibration,[6] redox reactions,[7] charging,[8] spin and phonon blockade,[9] polaron,[10] quantum interference,[11] misalignment of molecular orbitals,[12] etc. Most of the studies addressed short molecules with a linear backbone. Here we report our studies of single-molecule NDC effect in long molecular wires (~10 nm) with a nonlinear backbone. We find that nonlinear molecular backbones in polyporphyrin oligomer wires introduce NDC in resonant transport.[13] The first-principles simulations reveal that hybridization of the electrodes' continuum states with the resonant transport molecular orbital is modulated by changing the external bias in a narrow bias window (−1.3 to −1.9 V). As a result, the transmission is strongly suppressed at higher bias, leading to NDC.[14] Our findings exemplify how concerted action of electrode−molecule coupling, molecular orbital delocalization and external bias command charge transport in molecular junctions.

Polyporphyrin oligomer (ppo) wires with various backbone morphologies were synthesized via on-surface coupling of 5,15-bis(4-bromophenyl)-10,20-diphenylporphyrin (Br_2-TPP) (Figure 1a, inset) on a Au(111) surface.[15] Linear ppo wires were formed at 150 °C,[13] whereas branched wires (T-wire) and wires

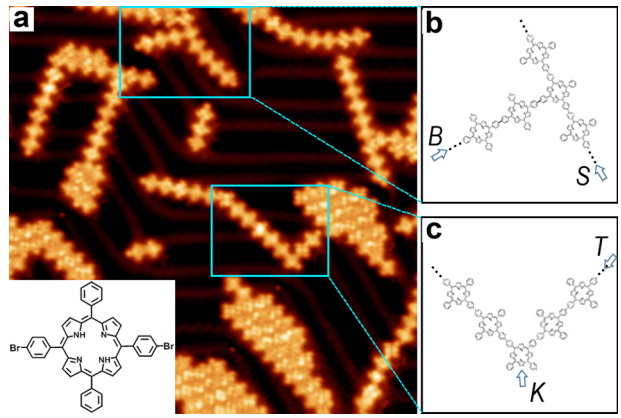

Figure 1. (a) STM topograph (40 × 40 nm) showing linear and nonlinear ppo wires synthesized on a Au(111) surface. Inset: Br_2-TPP. A T-wire and an L-wire are highlighted in the frames. (b, c) Corresponding chemical structures to the T-junction and the 90° kink.

with a 90° kink (L-wire) were formed at 200 °C (Figure 1a), presumably via dehydrogenation of the terminal phenyl moieties of Br_2-TPP. The chemical structures of the T-junction and the 90° kink are shown in Figure 1b,c, respectively. The various termini of the wires are denoted using letters ***B***, ***S***, ***K*** or ***T***.

To measure the single-molecule conductance through different transport paths, we used a scanning tunneling microscope tip to lift the wires at a selected terminus.[13,16] As illustrated in Figure 2a, we lifted a T-wire at its ***S*** terminus and measured conductance at various tip heights. (The corresponding scanning tunneling microscopy (STM) images of this T-wire acquired before and after manipulation and measurement are shown in Figure S1). Figure 2b shows differential conductance (dI/dV) acquired at five tip heights indicated as ΔZ (the corresponding $I-V$ traces are shown in Figure S1c). All five dI/dV traces feature a sharp peak. Except at the lowest tip height of ΔZ = 2.7 nm, the differential conductance

Received: October 17, 2017
Published: December 28, 2017

DOI: 10.1021/jacs.7b11016
J. Am. Chem. Soc. 2018, 140, 570−573

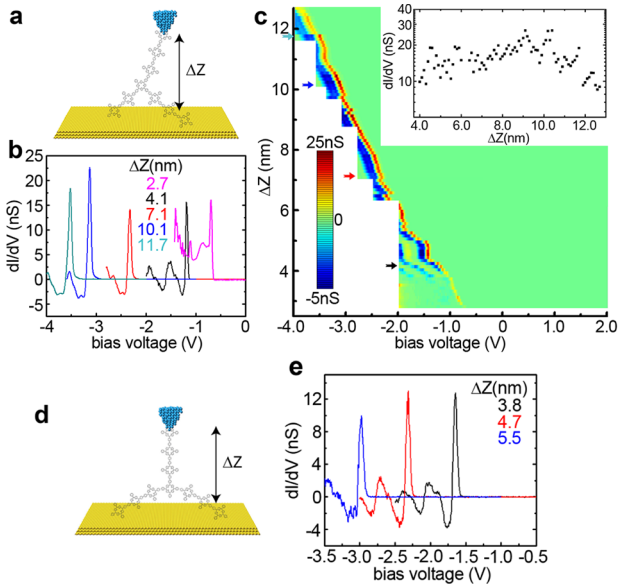

Figure 2. (a) Schematic illustration of T-wire transport lifted up at one of its ***S*** termini. (b) dI/dV traces of a T-wire in configuration (a) acquired at the indicated tip heights (the color code corresponds to the arrow of the same color in panel c). (c) Differential conductance against tip height. Inset: values of the first differential conductance peak plotted against tip height. (d) Schematic illustration of T-wire transport lifted up at its ***B*** terminus. (e) dI/dV traces of a T-wire in configuration (d) acquired at the indicated tip heights.

acquired at four higher tip heights exhibits clear NDC signatures, showing negative values right after the sharp peak. At 4.1 nm tip height, the conductance re-enters negative region after the first NDC regime. The multiple-peak feature was assigned to a vibronic effect.[13] We speculate the re-entering NDC is associated with the vibronic effect. The peaks are at increasingly negative bias as the tip height increased. This behavior is attributed to the fact that the effective bias voltage falling on the molecule in the metal−molecule−metal junction is a function of wire length.[13] Plotting series of dI/dV traces acquired at progressively increased tip heights on a color scale as a function of bias voltage (x axis) and tip height (y axis), as shown in Figure 2c, characterizes the tip-height dependent charge transport. This plot shows that the NDC regime is present above a tip height of 3.5 nm. In the inset in Figure 2c, the differential conductance peak values are plotted against tip height, displaying decay-less behavior from 4 to 11 nm. Apart from NDC, the T-wires display similar transport characteristics as the linear wires we reported previously,[13] suggesting that the sharp peak signifies resonant transport through a delocalized molecular orbital. We also lifted the ***B*** terminus of a T-wire, as illustrated in Figure 2d (the corresponding STM images of this T-wire acquired before and after manipulation and measurement are shown in Figure S2). As shown in Figure 2e, the differential conductance at different heights displays similar NDC features. We measured more than 20 T-wires and found all exhibit NDC when lifted at either ***B*** or ***S*** termini.

The fact that NDC is observed in the T-wires but not in the linear wires hints this effect is associated with the presence of T-junction, in other words, the nonlinear backbone. This may help explain why NDC is absent at tip heights below 3.5 nm (Figure 2b,c): at such low tip heights, the T-junction porphyrin unit was not lifted off the surface, so charge was not transported through the T-junction but through a linear backbone, thus showing the behavior of a linear wire. Here we propose two possible NDC mechanisms: (1) interference due to multiple transport pathways in the T-wires[11] or (2) transport through a nonlinear backbone.

To elucidate these two mechanisms, we investigated charge transport through L-wires. As illustrated in Figure 3a, when an

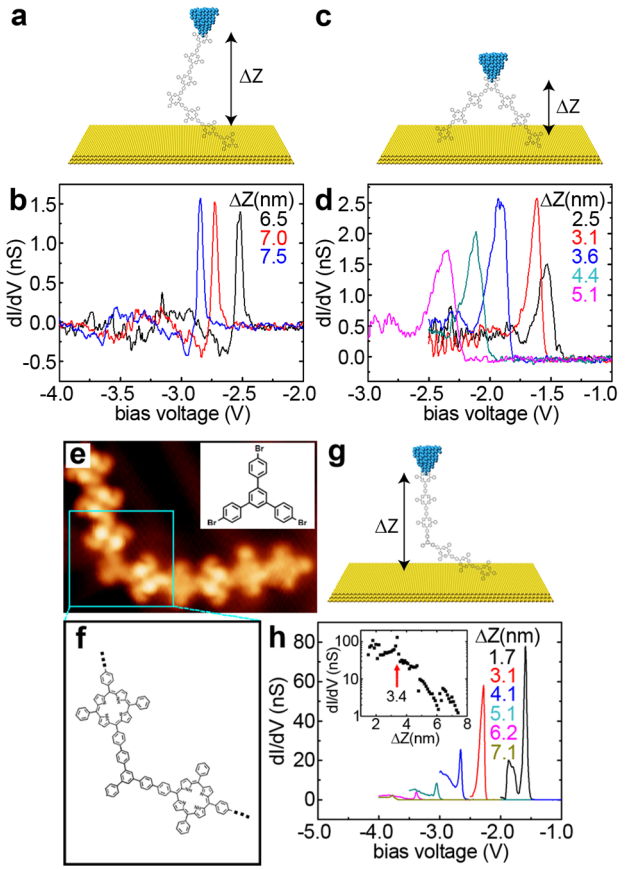

Figure 3. (a) Schematic illustration of L-wire transport lifted up at one of its ***T*** termini and (b) dI/dV traces of an L-wire acquired at the indicated tip heights. (c) Schematic illustration of L-wire transport lifted up at its ***K*** terminus and (d) dI/dV traces of an L-wire acquired at the indicated tip heights. (e) STM topograph (10 × 7.5 nm) of a V-wire (Inset: Br_3-TBB molecule) and (f) chemical structure of the 120° kink. (g) Schematic illustration of V-wire transport and (h) dI/dV traces of a V-wire acquired at the indicated tip heights. Inset: dI/dV peak values of the V-wire plotted against tip height.

L-wire is lifted up at its ***T*** terminus above a threshold height, conductance is through a 90° kink. Figure 3b shows that the measured conductance exhibits NDC features. Interestingly, about two-thirds of all the L-wires we successfully measured showed NDC while the rest one-third did not show NDC (Figure S3). It is worthwhile to note that when some L-wires were lifted and measured multiple times, NDC was present in some measurements but not in others. The L-wires feature a bistable NDC. We also lifted the L-wires at the ***K*** terminus (Figure S4), as illustrated by Figure 3c. This configuration permits two transport pathways. As shown in Figure 3d, dI/dV traces do not feature negative value and this result was obtained in all the L-wires examined. We conclude that this two-pathway transport configuration does not afford NDC. Therefore, we rule out that the NDC observed in the T-wires is associated

DOI: 10.1021/jacs.7b11016
J. Am. Chem. Soc. 2018, 140, 570−573

with multiple current pathways. Instead, we propose that the NDC is associated with bending or T-junction in the wire.

We reasoned that the bistable NDC in the L-wires may reflect an influence of bending angle of the kink because the bending angle could be changed in different manipulations conducted in our experiments. We calculated the frontier molecular orbitals of an L-shaped oligomer which consists of three porphyrin units. Its HOMO, HOMO-1 and HOMO-2 are delocalized (Figure S5). When the central kink is bent to 120°, its HOMO, HOMO-1 and HOMO-2 become localized (Figure S5). Therefore, stretching the kink angle of an L-shaped wire to 120° can significantly modify its transport characteristics. To test this idea experimentally, we synthesized V-shaped wires (V-wire) with a 120° kink by mixing Br_2-TPP with another precursor molecules 1,3,5-tris(4-bromophenyl)benzene (Br_3-TBB, as shown in inset of Figure 3e). Figure 3e,f shows the STM topograph of a V-wire and the chemical structure of the 120° kink. As illustrated in Figure 3g, we lifted the V-wire at one of its termini to measure the charge transport passing through the 120° kink. The representative differential conductance features sharp peaks but no NDC (Figure 3h). This finding corroborates our speculation that the bending angle of the kinks is decisive for NDC transport in the nonlinear wires. As plotted in Figure 3h inset, the differential conductance of the V-wire decays slowly when the tip height is below 3.4 nm, but much faster above 3.4 nm.

We performed first-principles nonequilibrium Green's function calculations to simulate the transport of two metal-molecule-metal junctions. As shown in Figure 4a, the junctions have a bottom electrode of flat Au substrate and a top electrode with a pyramid-shaped tip. The molecules in the junctions consist of two porphyrin units connected by a central porphyrin (right in Figure 4a) or TBB moiety (left in Figure 4a) to simulate the L-wire and the V-wire, respectively. Due to computation resource limitation, we did not simulate the T-wire. The frontier molecular orbitals (MOs) of the two molecules are shown in Figure S5. The 90°-kinked molecule features a delocalized HOMO−1 which provides a resonant transport channel and gives rise to the nearly decay-less conductance. The 120°-kinked molecule, however, does not possess any frontier MOs that are delocalized in the entire molecule. This can explain the conductance decay behavior presented in Figure 3h inset. When the tip height was below 3.4 nm, the TBB unit was still on the substrate, and the conductance was through a linear backbone, so the transport behavior is similar as the linear wires decaying slowly.[13] Above 3.4 nm tip height, the TBB unit was lifted off the substrate, and the conductance passed through the 120° kink. In this configuration, resonant transport did not work because of lacking of delocalized MO, so the conductance decayed exponentially with increasing tip height.

Figure 4b shows the simulated differential conductance (Inset: $I-V$ traces) of the two junctions. NDC is present in the 90°-kinked junction but not in the 120°-kinked junction, corroborating the experimental observations. The transmission map of the 90°-kinked junction is plotted in Figure 4c. It reveals that as HOMO-1 entering the conductance window at −1.2 and +1.3 V (as marked by the arrows in Figure 4c), the current increases abruptly. So, the differential conductance peaks in Figure 4b are due to the resonant transport afforded by HOMO-1. The transmission of HOMO-1 becomes weaker when further increasing the bias voltage beyond −1.5 or +1.5 V, which results in current reduction and NDC effect.

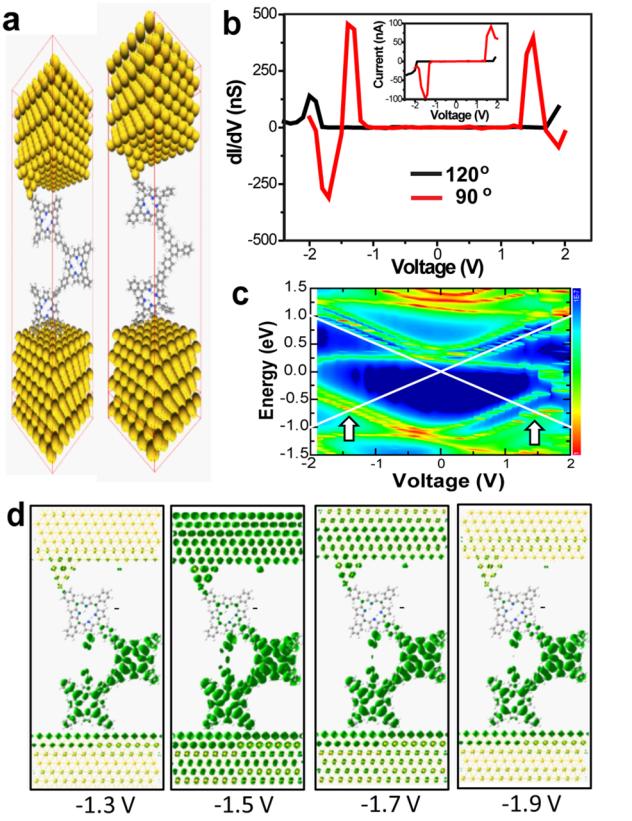

Figure 4. (a) Metal−molecule−metal junctions containing a 90°-kink (left) and a 120°-kink (right). (b) Simulated differential conductance of the two junctions. Inset: simulated $I-V$ traces. (c) Transmission map of the 90°-kinked junction. The white crosses indicate the conductance window. (d) Density of states of HOMO-1 of the 90°-kink junction at the indicated bias.

To understand the underlying mechanism of the reduced transmission, we plot the density of states (DOS) distribution of HOMO-1 at four tip−substrate bias (−1.3, −1.5, −1.7, and −1.9 V) in Figure 4d. The DOS at the molecule remains largely unchanged at the four biases, suggesting that the NDC is not associated with the bias-induced changes in molecular orbitals. The DOS of the electrodes is very different in the four maps. At −1.5 V, the DOS is very strong at the two electrodes, indicating HOMO-1 hybridizes effectively with the states of the two electrodes. In comparison, the DOS at the two electrodes is reduced at −1.7 V and become even weaker at −1.9 V. The degree of hybridization between the resonant transport MO and electrode continuum states is strongest at −1.5 V and weakened significantly at higher bias. In contrast, similar analysis (Figure S6) of a junction containing a linear oligomer, which does not exhibit NDC, reveals that such bias-modulated hybridization does not occur. Given that coupling strength dictates transmission of the junction,[3a] we suggest that the weakened coupling at higher bias introduces NDC effect in the 90°-kinked junction.

In summary, combining on-surface synthesis and single-molecule manipulation technique, we are able to correlate the conductance characteristics with charge transport paths in molecular wires. NDC was observed in the wires with T-shape and L-shape backbones, but not linear or 120° kinked backbones. The simulations uncover a concerted NDC mechanism: (1) the molecular backbone dictates a molecular

DOI: 10.1021/jacs.7b11016
J. Am. Chem. Soc. 2018, 140, 570−573

orbital that can serve as a resonant charge transport channel; and (2) the coupling strength between this molecular orbital and the electrodes is strongly modulated by the external bias, specifically, weakened at higher bias. We anticipate this mechanism can be at work in a broad range of molecular junctions.

■ ASSOCIATED CONTENT

Supporting Information

The Supporting Information is available free of charge on the ACS Publications website at DOI: 10.1021/jacs.7b11016.

Methods and supporting figures (PDF)

■ AUTHOR INFORMATION

Corresponding Authors

*phnlin@ust.hk
*keqiuchen@hnu.edu.cn
*liupn@ecust.edu.cn

ORCID

Shi Zhang Chen: 0000-0003-4218-4808
Linghao Yan: 0000-0002-4860-8096
Pei Nian Liu: 0000-0003-2014-2244
Nian Lin: 0000-0001-5693-4011

Author Contributions

G. Kuang and S.-Z. Chen contributed equally to this work.

Notes

The authors declare no competing financial interest.

■ ACKNOWLEDGMENTS

This research was supported by Hong Kong RGC (No. 6301415), N_HKUST601/15 and National Natural Science Foundation of China (Nos. 11674092 and 21561162003).

■ REFERENCES

(1) Esaki, L. *Phys. Rev.* **1958**, *109*, 603.
(2) Sollner, T.; Goodhue, W. D.; Tannenwald, P. E.; Parker, C. D.; Peck, D. D. *Appl. Phys. Lett.* **1983**, *43*, 588.
(3) (a) Moth-Poulsen, K.; Bjornholm, T. *Nat. Nanotechnol.* **2009**, *4*, 551. (b) Wang, K.; Xu, B. *Top. Curr. Chem.* **2017**, *375*, 17.
(4) Xue, Y. Q.; Datta, S.; Hong, S.; Reifenberger, R.; Henderson, J. I.; Kubiak, C. P. *Phys. Rev. B: Condens. Matter Mater. Phys.* **1999**, *59*, R7852.
(5) (a) Shi, X. Q.; Zheng, X. H.; Dai, Z. X.; Wang, Y.; Zeng, Z. *J. Phys. Chem. B* **2005**, *109*, 3334. (b) Capozzi, B.; Low, J. Z.; Xia, J. L.; Liu, Z. F.; Neaton, J. B.; Campos, L. M.; Venkataraman, L. *Nano Lett.* **2016**, *16*, 3949. (c) Huang, J.; Xu, K.; Lei, S. L.; Su, H. B.; Yang, S. F.; Li, Q. X.; Yang, J. L. *J. Chem. Phys.* **2012**, *136*, 064707.
(6) Gaudioso, J.; Lauhon, L. J.; Ho, W. *Phys. Rev. Lett.* **2000**, *85*, 1918.
(7) (a) Chen, J.; Reed, M. A.; Rawlett, A. M.; Tour, J. M. *Science* **1999**, *286*, 1550. (b) Chen, J.; Wang, W.; Reed, M. A.; Rawlett, A. M.; Price, D. W.; Tour, J. M. *Appl. Phys. Lett.* **2000**, *77*, 1224. (c) Xiao, X. Y.; Nagahara, L. A.; Rawlett, A. M.; Tao, N. J. *J. Am. Chem. Soc.* **2005**, *127*, 9235. (d) Mentovich, E. D.; Kalifa, I.; Tsukernik, A.; Caster, A.; Rosenberg-Shraga, N.; Marom, H.; Gozin, M.; Richter, S. *Small* **2008**, *4*, 55. (e) Kiehl, R. A.; Le, J. D.; Candra, P.; Hoye, R. C.; Hoye, T. R. *Appl. Phys. Lett.* **2006**, *88*, 172102. (f) Le, J. D.; He, Y.; Hoye, T. R.; Mead, C. C.; Kiehl, R. A. *Appl. Phys. Lett.* **2003**, *83*, 5518.
(8) Kratochvilova, I.; Kocirik, M.; Zambova, A.; Mbindyo, J.; Mallouk, T. E.; Mayer, T. S. *J. Mater. Chem.* **2002**, *12*, 2927.
(9) Heersche, H. B.; de Groot, Z.; Folk, J. A.; van der Zant, H. S. J.; Romeike, C.; Wegewijs, M. R.; Zobbi, L.; Barreca, D.; Tondello, E.; Cornia, A. *Phys. Rev. Lett.* **2006**, *96*, DOI: 10.1103/PhysRevLett.96.206801.
(10) Kang, N.; Erbe, A.; Scheer, E. *Appl. Phys. Lett.* **2010**, *96*, 023701.
(11) (a) Kang, N.; Erbe, A.; Scheer, E. *Appl. Phys. Lett.* **2010**, *96*, 023701. (b) Galperin, M.; Ratner, M. A.; Nitzan, A. *Nano Lett.* **2005**, *5*, 125.
(12) (a) Majima, Y.; Ogawa, D.; Iwamoto, M.; Azuma, Y.; Tsurumaki, E.; Osuka, A. *J. Am. Chem. Soc.* **2013**, *135*, 14159. (b) Perrin, M. L.; Frisenda, R.; Koole, M.; Seldenthuis, J. S.; Gil, J. A. C.; Valkenier, H.; Hummelen, J. C.; Renaud, N.; Grozema, F. C.; Thijssen, J. M.; Dulic, D.; van der Zant, H. S. J. *Nat. Nanotechnol.* **2014**, *9*, 830. (c) Fan, W.; Zhang, R. Q.; Rocha, A. R.; Sanvito, S. *J. Chem. Phys.* **2008**, *129*, 074710.
(13) Kuang, G.; Chen, S.-Z.; Wang, W.; Lin, T.; Chen, K.; Shang, X.; Liu, P. N.; Lin, N. *J. Am. Chem. Soc.* **2016**, *138*, 11140.
(14) Liu, Z.-F.; Neaton, J. B. *J. Phys. Chem. C* **2017**, *121*, 21136.
(15) (a) Grill, L.; Dyer, M.; Lafferentz, L.; Persson, M.; Peters, M. V.; Hecht, S. *Nat. Nanotechnol.* **2007**, *2*, 687. (b) Adisoejoso, J.; Lin, T.; Shang, X. S.; Shi, K. J.; Gupta, A.; Liu, P. N.; Lin, N. *Chem. - Eur. J.* **2014**, *20*, 4111.
(16) (a) Lafferentz, L.; Ample, F.; Yu, H.; Hecht, S.; Joachim, C.; Grill, L. *Science* **2009**, *323*, 1193. (b) Koch, M.; Ample, F.; Joachim, C.; Grill, L. *Nat. Nanotechnol.* **2012**, *7*, 713. (c) Nacci, C.; Ample, F.; Bleger, D.; Hecht, S.; Joachim, C.; Grill, L. *Nat. Commun.* **2015**, *6*, 7397. (d) Reecht, G.; Scheurer, F.; Speisser, V.; Dappe, Y. J.; Mathevet, F.; Schull, G. *Phys. Rev. Lett.* **2014**, *112*, 112. (e) Chong, M. C.; Reecht, G.; Bulou, H.; Boeglin, A.; Scheurer, F.; Mathevet, F.; Schull, G. *Phys. Rev. Lett.* **2016**, *116*, DOI: 10.1103/PhysRevLett.116.036802. (f) Nacci, C.; Viertel, A.; Hecht, S.; Grill, L. *Angew. Chem., Int. Ed.* **2016**, *55*, 13724.

DOI: 10.1021/jacs.7b11016
J. Am. Chem. Soc. 2018, 140, 570−573